Available online at www.sciencedirect.com
SCIENCE DIRECT®
International Journal of Heat and Fluid Flow 25 (2004) 384–392
International Journal of HEAT AND FLUID FLOW
www.elsevier.com/locate/ijhff

# Structure of turbulent channel flow with square bars on one wall

S. Leonardi [a,*], P. Orlandi [a], L. Djenidi [b], R.A. Antonia [b]

[a] Dipartimento di Meccanica e Aeronautica, University of Rome "La Sapienza", 00184 Rome, Italy
[b] Discipline of Mechanical Engineering, University of Newcastle, NSW 2308, Australia

**Abstract**

The organised motion in a turbulent channel flow with a succession of square bars on the bottom wall has been investigated using direct numerical simulations. Several values of the ratio $w/k$, where $k$ is the bar height and $w$ is the longitudinal separation between consecutive bars have been examined in detail. Relative to a smooth surface, the streamwise extent of the near-wall structures is decreased while their spanwise extent is increased. As $w/k$ increases, the coherence decreases in the streamwise direction having a minimum for $w/k = 7$. This is due to the outward motion occurring, most of all, near the leading edge of the elements. The Reynolds stress anisotropy tensor and its invariants show a closer approach to isotropy over the rough wall than over a smooth wall.


*Keywords:* Turbulence; Roughness

## 1. Introduction

Since the pioneering work of Kline et al. (1967), a wealth of information is now available on the structure of a turbulent boundary layer on a smooth wall (e.g. Cantwell, 1981; Robinson, 1991). Much less is known on a turbulent boundary layer over rough surfaces. In particular, the effect the roughness has on the near-wall structure of the boundary layer is far from complete. This is in part related to the poor reliability of measurements in the vicinity of the roughness. Further, the number of parameters that affect the flow, (for example the density, height, shape of the roughness as well as its nature, e.g. 2D or 3D) compounds these difficulties. Nevertheless, useful results have emerged from experimental studies on the way low-speed streaks are modified by the roughness. The flow visualizations of Grass et al. (1993) over a rough wall made up of spheres indicated that the distance between the streaks increased, whereas their streamwise coherence was reduced relative to a smooth wall. Consistently, Krogstad and Antonia (1994) found that two-point correlations over a mesh roughness indicated a decrease in streamwise correlation with a slight increase in the spanwise extent of the structures. Different features are observed over a particular (so-called "d-type") rough wall made up of square bars transverse to the flow, with $w/k = 1$ (e.g. Perry et al., 1969; Wood and Antonia, 1975; Djenidi et al., 1999). For a d-type roughness, the latter authors found low and high-speed streaks alternating in the spanwise direction with approximately the same normalised spacing as over a flat wall. All these results are relative to the fully rough regime. Ashrafian and Anderson (2003) have carried out a DNS of the turbulent channel flow, with transverse square bars, in the transitional regime ($k^+ \simeq 13$). They showed that streaky structures are only weakly affected by the rough walls.

A systematic study of the changes caused by varying $w/k$ has yet to be attempted in experiments. In a previous paper the dependence of the roughness function on $w/k$ was discussed (Leonardi et al., 2003), here we use direct numerical simulations to examine how this ratio influences the organised structures near the wall. In particular, we consider two-point velocity correlations, with the fixed point at several locations within one roughness wavelength. We also consider the effect $w/k$ has on the way the cavity communicates with the overlying flow. The departure from isotropy of the Reynolds stress tensor is also examined in the context of its anisotropy invariants.

* Corresponding author. Tel.: +39-0644-585556; fax: +39-0648-4854.
*E-mail address:* leonardi@kolmogorov.ing.uniroma1.it (S. Leonardi).

0142-727X/$ - see front matter © 2004 Published by Elsevier Inc.
doi:10.1016/j.ijheatfluidflow.2004.02.022

## 2. Numerical procedure

The non-dimensional Navier–Stokes and continuity equations for incompressible flows are:

$$\frac{\partial U_i}{\partial t}+\frac{\partial U_i U_j}{\partial x_j}=-\frac{\partial P}{\partial x_j}+\frac{1}{Re}\frac{\partial^2 U_i}{\partial x_j^2}+\Pi,\quad \nabla\cdot U=0 \qquad (1)$$

where $Re=(U_c h/\nu)$ is the Reynolds number, $h$ is the channel half-width, $U_c$ is the centreline laminar Poiseuille velocity, $\nu$ is the kinematic viscosity, $\Pi$ is the pressure gradient required to maintain a constant flow rate, $U_i$ is the component of the velocity vector in the $i$ direction and $P$ is the pressure. The Navier–Stokes equations have been discretized in an orthogonal coordinate system using staggered central second-order finite-differences. Here, only the main features are recalled since details of the numerical method can be found in Orlandi (2000). The discretized system is advanced in time using a fractional-step method with viscous terms treated implicitly and convective terms explicitly. The large sparse matrix resulting from the implicit terms is inverted by an approximate factorisation technique. At each time step, the momentum equations are advanced with the pressure at the previous step, yielding an intermediate non-solenoidal velocity field. A scalar quantity $\Phi$ projects the non-solenoidal field onto a solenoidal one. A hybrid low-storage third-order Runge–Kutta scheme is used to advance the equations in time. The roughness is treated by the efficient immersed boundary technique described in detail by Fadlun et al. (2000). This approach allows the solution of flows over complex geometries without the need of computationally intensive body-fitted grids. It consists of imposing $U_i=0$ on the body surface which does not necessarily coincide with the grid.

## 3. Flow configuration

DNSs have been performed for a fully developed turbulent channel flow with square bars on the bottom wall. Several values of $w/k$ within of the larger database (0.33, 0.6,1, 2.07, 3, 4, 5.5, 7, 8, 9, 10, 19, 39, Leonardi et al., 2003) have been investigated in more detail, with particular emphasis on the correlations. Periodic boundary conditions apply in the streamwise ($x$) and spanwise ($z$) directions, and there is a no slip condition at the wall. The computational box is $8h\times 2h\times \pi h$ in $x$, $y$ (wall-normal direction) and $z$, respectively (Fig. 1), the roughness height is $k=0.2h$. The Reynolds number is $Re=4200$ and corresponds to $h^+=180$ when both walls are smooth. The superscript "+" denotes normalisation by wall units $U_\tau(\equiv(\tau/\rho)^{1/2})$, $\tau$ is the wall shear stress equal to the sum per unit area of the skin frictional drag and form drag. The flow rate has been kept constant in all simulations, hence $U_\tau$, $k^+$ and $h^+$ depend on $w/k$. Results pertaining to the pressure and friction along the wall, and the Clauser roughness function may be found in Leonardi et al. (2003). The simulations also focused on the dependence of the viscous drag ($D_v$) and form drag ($D_P$) on the ratio $w/k$. It was observed that, as $w/k$ increased, $D_P$ increased, reaching a maximum for $w/k\approx 7$. For this $w/k$, $D_v$ was minimum. Such a behaviour implies that structural changes occur as $w/k$ varies.

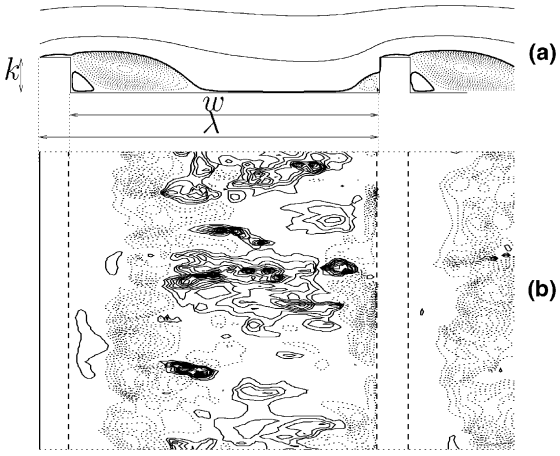


Fig. 1. Square bar roughness, $w/k=10$. Top: mean streamlines, averaged with respect to time and $z$. Bottom: instantaneous $1/Re\,\partial u/\partial y$ on the bottom wall. The thick line corresponds to the zero streamfunction (top) and to $u=0$ (bottom). (—) positive, (- - -) negative. The definitions of $k$, $w$ and $\lambda$ are indicated. Flow is from left to right.

## 4. Mean flow

Mean streamlines have shown that for $w/k<7$, separation occurs at the trailing edge of the element and reattachment is on the opposite vertical wall (Leonardi et al., 2003). For $w/k\geqslant 7$ (Fig. 1a), the flow reattaches on the bottom wall. As the next element is approached, the streamlines are tilted upward and a new separation region is formed. Fig. 1b shows the instantaneous skin friction coefficient $C_f=1/Re\,\partial u/\partial y$ on the bottom wall for the case $w/k=10$. The reattachment and separation points ($C_f=0$) vary in time and spanwise direction (Fig. 1). This is in agreement with the visualizations performed by Liu et al. (1966), with the DNS of a turbulent flow over a backward facing step by Le et al. (1997) and with the LES by Cui et al. (2003). Fig. 2 shows distributions of $\overline{U}^+$ for a wide range of $w/k$ and the smooth channel flow distribution of Kim et al. (1987) is included as reference (here an overbar denotes averaging with respect to time $x$ and $z$). The origin in $y$ was found by fitting the velocity profiles to $\overline{U}^+=(1/0.41)\ln y^+ + C'$. As expected, the velocity exhibits a downward shift with respect to the smooth channel. The maximum shift occurs at $w/k=7$, i.e. the geometry which yielded the

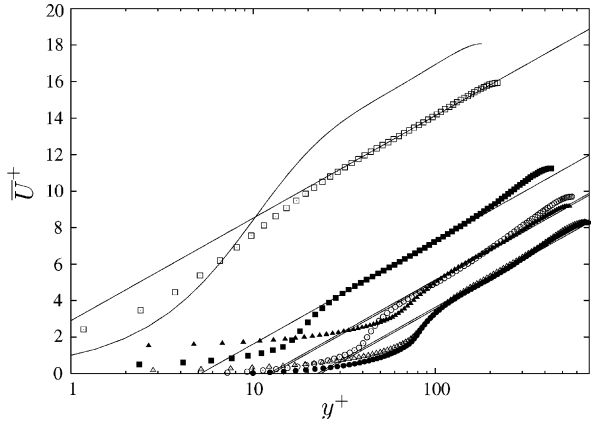


Fig. 2. Distributions of $\overline{U}^+$. (—) Kim et al. (1987). (□) $w/k = 1$; (■) $w/k = 3$; (○) 4; (●) 7; (△) 9; (▲) 19. The solid lines of reference are $\overline{U}^+ = 1/0.41 \ln y^+ + C'$, $C'$ being 2.9, −4, −6.2, −7.7, −7.6, −6.1 for $w/k = 1$, 3, 4, 7, 9, 19, respectively.

maximum value of form drag. For large values of $w/k$, the velocity profiles gradually return to the smooth wall case.

Ashrafian and Anderson (2003), and Bakken and Krogstad (2003) have investigated turbulent channel flows with roughness on both the walls. A symmetrical configuration is useful for experimentalists because $U_\tau$ can be calculated from the pressure drop. On the other hand, numericists can obtain $U_\tau$ simply by integrating the pressure and friction distribution on the wall. Therefore, numericists can avoid to treat roughness on the upper wall which presents an extra cost in term of number of points and computational time. However, it would certainly be of interest to know how the presence of the upper wall roughness affects the flow near the bottom wall. To this end, we carried out, for $w/k = 3$, another simulation with square elements on both walls (Fig. 3). The recirculation within the cavities compares well with that reported in Leonardi et al. (2003) with square elements placed on the bottom wall only. Pressure and skin friction distributions (along the bottom wall) are also in close agreement between the two cases (Fig. 4).

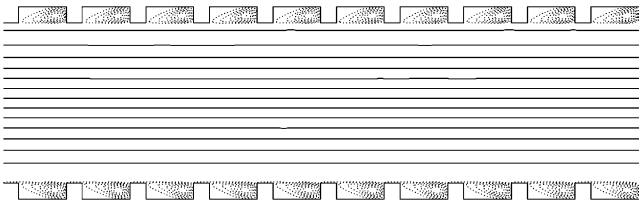

Fig. 3. Geometrical sketch and streamlines of a turbulent channel flow with square elements on the both walls ($w/k = 3$).

With roughness on both walls, the velocity profile is, as expected, symmetric while, when roughness is only on the bottom wall, the maximum of $\overline{U}$, $y_{\max}$, is shifted upward. However, when $\overline{U}$ is scaled in wall units, the two profiles overlap and the value of the roughness function is independent of the boundary condition on the upper wall. Visualizations for the two cases, (not shown here), reveal the same.

## 5. Streaks and two-point correlations

The turbulent boundary layer over a flat wall is characterised by elongated streaks which lift up in a pseudo-random manner before breaking down. To assess the effect of the roughness, we compare instantaneous fluctuations of the streamwise velocity ($u/u'$), (where a prime denotes an rms value) in horizontal planes ($x$–$z$), at $y/h = 0.03$ (for a flat channel, at this Reynolds number this distance would correspond to $y^+ \simeq 6$). For $w/k = 1$, the streaks start to be disrupted. However, elongated structures, somewhat shorter than those over a smooth wall, can be noted (Fig. 5b). These resemble those in the visualizations of Djenidi et al. (1999) for the same surface. By increasing $w/k$ (Fig. 5c and d), the fluctuations increase in magnitude with a maximum for $w/k = 7$ (minimum and maximum are −0.28, 0.37; −0.49, 0.5; −0.63, 0.66; −0.59, 0.65 for $w/k = 1$, 3, 7, 19, respectively). This is due to the increased momentum exchange with the outer layer, as previously noted from a quadrant analysis by Krogstad et al. (1992). The structures, with a loss of coherence in

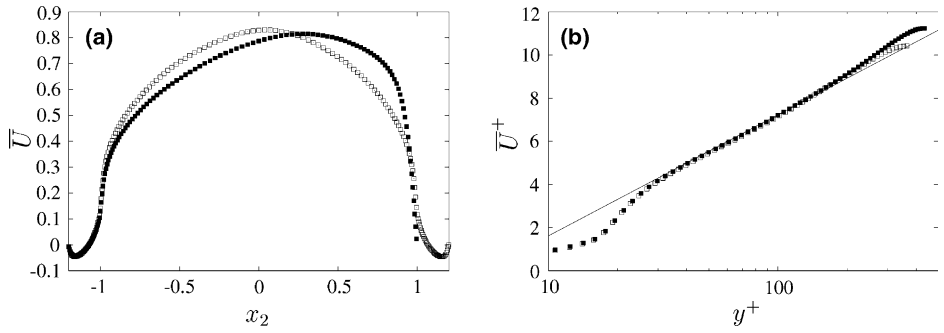


Fig. 4. Comparison of the mean velocity profiles, for $w/k = 3$: (□) roughness on both walls, (■) roughness on the bottom wall.

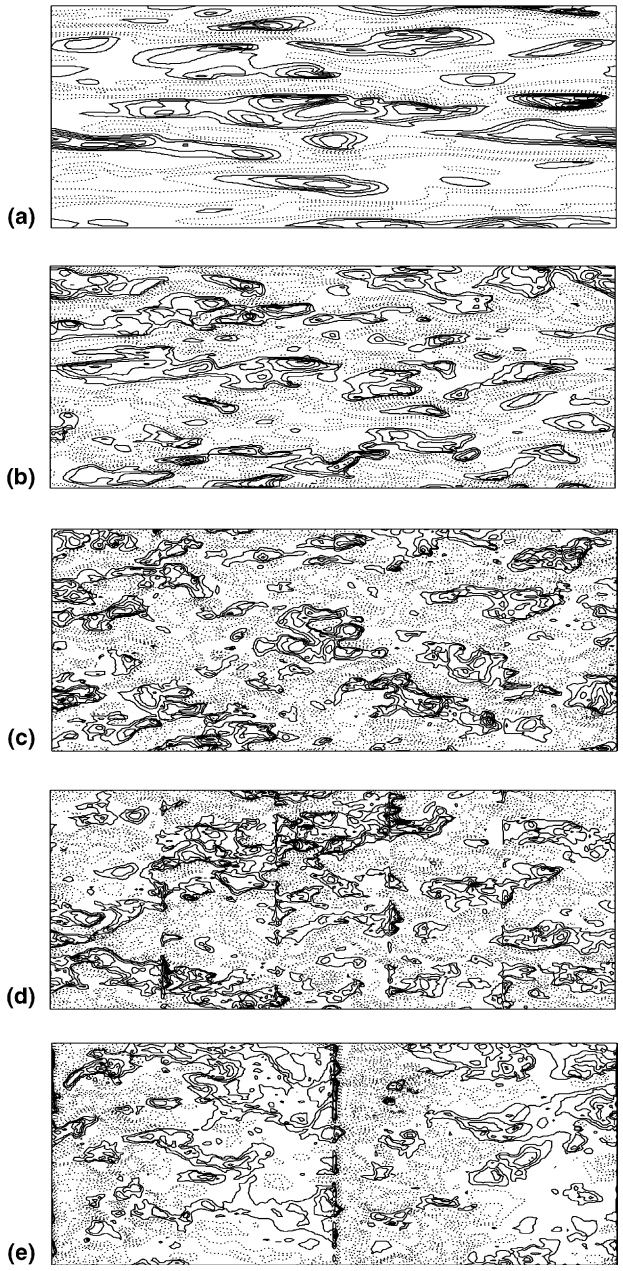


Fig. 5. Contour plots of $u/u'$, where a prime denotes an rms (—) positive, (···) negative. (a) Smooth channel, (b) $w/k = 1$ (c) 3, (d) 7, (e) 19. Increment 0.5.

$x$, tend to be more isotropic than in the smooth wall case. Very close to the plane of the crest (not shown here), the roughness splits the elongated structures into nearly circular regions located above the grooves. The no-slip condition ($u = 0$) on the crests reduces the coherence in the streamwise direction and produces $\partial u/\partial x$. Moreover within the cavity, near the leading edge of the element, $\partial u/\partial x < 0$. Continuity requires $\partial u/\partial x$ to be balanced by $\partial v/\partial y$ and $\partial w/\partial z$ ($v$ and $w$ are the fluctuations of normal and spanwise velocity, respectively), thus leading to an enhancement of $v$ and $w$ near the rough wall.

To quantify the previous observations, two-point correlations, with one point fixed, were computed. Fig. 6 shows $\rho_{uu}(x_0, x, z) = \overline{u(\mathbf{x_0}, \mathbf{x})u(\mathbf{x})}/(u'(\mathbf{x_0})u'(\mathbf{x}))$ for $w/k =$ 1, 3, 7 in horizontal planes $(x, z)$. For reference, the smooth wall contours are included at the top of the figure. The overbar indicates averaging with respect to the number of fields and wavelength, (i.e. $\bar{u} = \sum_{n,t,z} u(x + n\lambda, t, z)$), $\mathbf{x}_0 = (x_0, y_0, z_0)$ are the coordinates of the fixed point, $\mathbf{x} = (x_0 + \Delta x, y_0, z_0 + \Delta z)$ is the position of the other point. Results were obtained at the same $y$ as the previous figures for 3 different $x_0$: on the crest ($x_a$, dashed line), at the centre of the cavity ($x_b$, dotted line), and slightly upstream of a roughness element ($x_c$, dashed dotted line). A decreased streamwise coherence, relative to the smooth wall case, is observed for all the rough surfaces. For $w/k = 1$, although the contours are considerably less elongated than over the smooth wall, the coherence in $x$ is larger than for the other surfaces investigated. However, from the present results, at this $k^+$, the disturbance to the overlying flow caused by the square grooves is not small. This is a confirmation that DNS complements the experiments and provides deeper insight into the physics of rough-wall flows. This can be better appreciated by considering $\rho_{uu}$ contours in the $(x, y)$-plane. Although they remain nearly as elongated as over the smooth wall, there is little doubt that their inclination has increased, underlying the increased communication between the cavities and the overlying flow (Fig. 7). The increased inclination

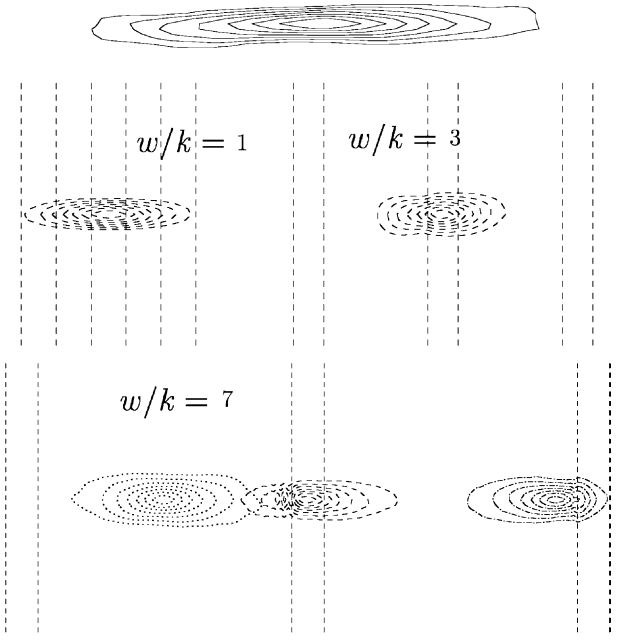


Fig. 6. Two-point correlation coefficients in the $(x, z)$-plane $\rho_{uu}(\mathbf{x_0})$, $y^+ = 6$. Contour from 0.3 to 1 (increment is 0.1). Left, $(w/k = 1)$; centre $(w/k = 3)$; right, $(w/k = 7)$. (- - -) $x = x_a$; (···) $x = x_b$; (–·–) $x = x_c$. Flow is left to right.

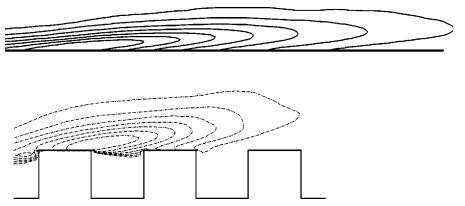

Fig. 7. Two-point correlation coefficient in the $(x,y)$-plane ($\rho_{uu}$, 0) at $y^+ = 6$. Contours are from 0.3 to 1 (increment is 0.1); top smooth wall, bottom $w/k = 1$.

is also consistent with the reduced streamwise correlation over this surface in Fig. 6.

As the distance from the wall increases, the extent of the streamwise correlation remains shorter than in the smooth channel. This can be inferred from the Taylor microscale $\lambda_x = (-0.5f''(0))^{0.5}$, where $f(r)$ is the longitudinal autocorrelation function, statistics are computed in $z$, $t$. Fig. 8 compares the Taylor microscale between smooth and rough walls. In the centre of the channel the distribution relative to the smooth channel, has a weak asymmetry, due probably to an insufficient number of samples. Indeed this is the region where the large scales act, and their convergence is much slower. In general, the effect of roughness is to shorten $\lambda_x$. Only for $w/k = 1$, there is a local peak near the rough wall ($x_2/h = -1$, with the origin of $x_2$ at the centerline). However the intensity is about half that on the smooth wall. This underlines once again that $w/k = 1$ is not a small disturbance. For $x_2/h > -0.5$, $\lambda_x$ is very close to that in the smooth channel. The smallest value of $\lambda_x$ is obtained for $w/k = 7$. For this geometry the Taylor microscale is the smallest almost everywhere across the channel. For larger values of $w/k$, $\lambda_x$ gradually returns to the values corresponding to the smooth wall (see for example $w/k = 39$).

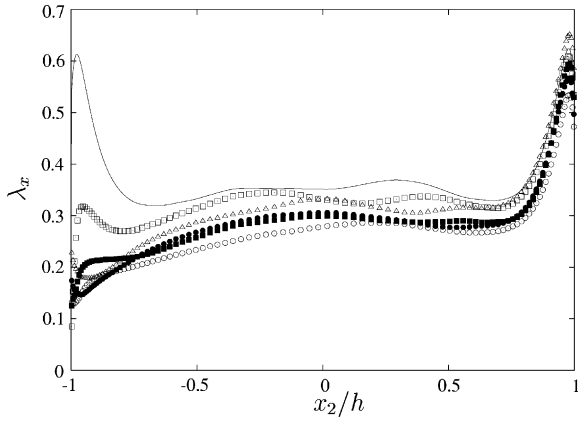


Fig. 8. Taylor microscale. (—) smooth wall, $w/k = 1$ (□), 3 (■), 7 (○), 19 (●), 39 (△).

The reduced $x$ extent of the correlation is accompanied by a lengthening in the $z$ extent. The correlation in the spanwise direction,

$$R_{u,u}(\Delta z, y) = \overline{u(x,y,z)u(x,y,z+\Delta z,t)}$$

has a minimum at about $z^+ = 50$ for $w/k = 1$ as in the smooth wall case (Fig. 9a). For larger values of $w/k$ $(3,7)$, $R_{u,u}$ gradually decreases in $z$ with a weaker minimum, about half than that of a smooth wall, shifted toward larger $\Delta z^+$ (138 and 210 for $w/k = 3$ and 7, respectively). This means that the structures are larger in $z$ and confirm the tendency toward isotropization. Moreover the decreased intensity of the minimum means that the alternating positive and negative signed structures, which are characteristic of smooth walls, are less frequent. As $u_\tau$ depends strongly on $w/k$, the correlation is shown also with respect to $\Delta z/h$ (Fig. 9b). The zero crossing of the correlation, $R_{u,u} = 0$ increases by increasing $w/k$ and has a maximum for $w/k = 7$. However the difference between $w/k = 3$ and 7 is small and amplified when the distance is normalised using wall units, (recall that $u_\tau$ is larger for $w/k = 7$).

For very large values of $w/k$, the flow tends to that over a smooth wall and then streaky structures are expected to appear on the bottom wall. This has been

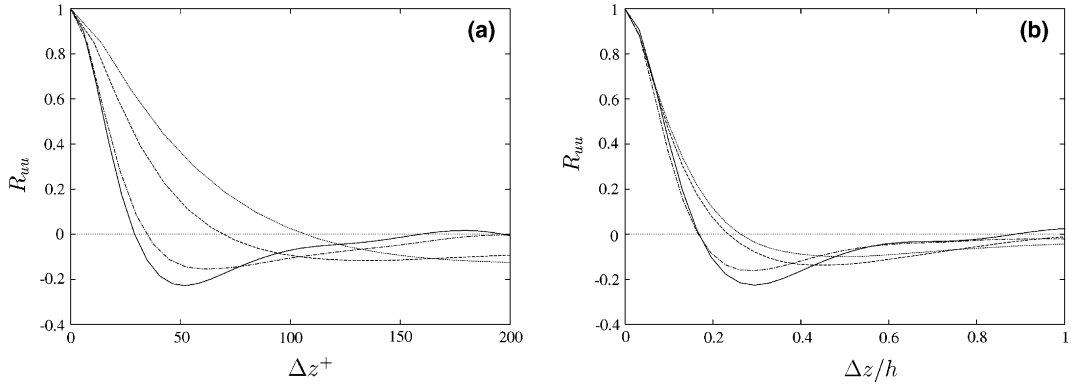


Fig. 9. Two-point correlation coefficients at $y^+ \simeq 10$ in spanwise direction. (—) smooth wall; (– – –) $w/k = 1$; (- - -) $w/k = 3$; (· · ·) $w/k = 7$. Figure (a) is a zoom *of* figure (b) in wall units.

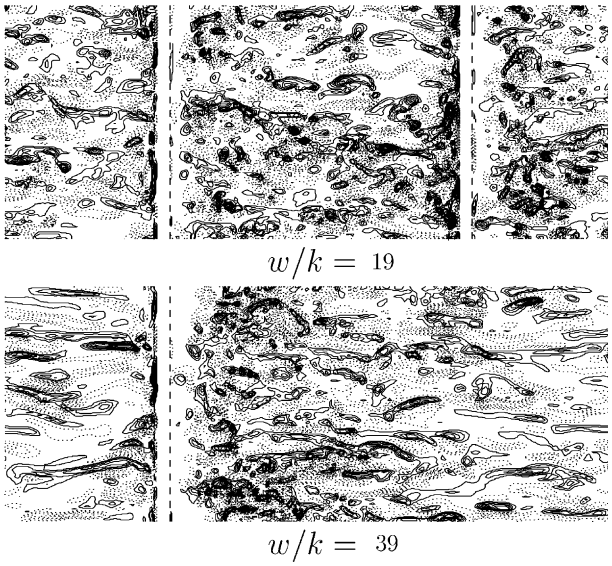


Fig. 10. Contours of instantaneous normal vorticity in $x$-, $z$-planes, at $\Delta y^+ \simeq 12$ from the bottom wall. Increments 0.5 (—) positive, (···) negative.

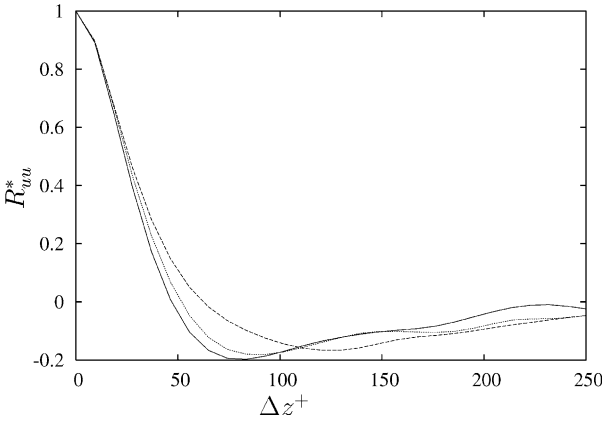


Fig. 11. Two-point correlation coefficients at $y^+ \simeq 10$ from the bottom wall, at different positions in $x$ for $w/k = 39$. (- - -), $32k$ (···), $37k$ (—), $38k$ downstream of the element.

corroborated by analysing instantaneous normal vorticity visualizations, in horizontal planes, at about 12 wall units from the bottom wall (Fig. 10). The roughness element produces a very strong disturbance which, locally, gives rise to short structures not aligned to the flow direction. Moving downstream from the leading edge, the vorticity tubes appear to be more and more aligned: however, for $w/k = 19$, the distance between the elements is too small and the coherence is disrupted once again by the subsequent obstacle. On the other hand, for $w/k = 39$, positive and negative vorticity tubes can be observed alternately in the spanwise direction, near the downstream end of the cavity, i.e. as the leading edge of the following element is neared (recall that the domain is periodic).

The previous discussion is quantified by two-point correlation coefficients in $z$, $R^*_{u,u}(\Delta z, y_0) = \overline{u(x_0, y_0, z)u(x_0, y_0, z + \Delta z, t)}$. Statistics, here, are calculated only in time and $z$, $x_0$ is kept fixed. As the leading edge of the downstream element is approached (moving away from the upstream element), the correlation coefficient becomes more and more negative, with the minimum occurring for smaller $\Delta z^+$. At about $38k$ downstream the element, the minimum is at $\Delta z^+ = 75$, therefore quite close to the smooth wall case (50), and much smaller than the values we found for $w/k = 3$ and 7 (Fig. 11).

## 6. Normal wall velocity

The changes in the correlations are attributable to the normal-wall motion induced by the roughness elements. Fig. 12 shows instantaneous contours of normal velocity near the leading edge of an element. For $w/k = 1$ the wall-normal velocity is very weak and this is, indeed, the case closer to the smooth wall. Nonetheless, the $v$ disturbance is probably still sufficient to cause the reduction in the $x$ extent of the correlation (as discussed earlier). As $w/k$ increases, the vertical motion becomes increasingly important, and reaches its maximum intensity for $w/k = 7$. In particular for the latter case very intense ejections ($v > 0$) can be observed on the plane of the crests. Therefore, when the flow approaches a roughness element, vertical and spanwise velocities are induced and interact with the overlying flow, modifying the structures.

The disturbance due to the roughness, has a periodicity in $x$ as is reflected in the correlation of the wall-normal velocity fluctuations. Local peaks of $R_{vv}$ occur with a separation equal to $\lambda$ for $w/k \geqslant 3$ (Fig. 13). However, for $w/k \geqslant 7$, the local minimum and maximum are more pronounced, implying a greater strength

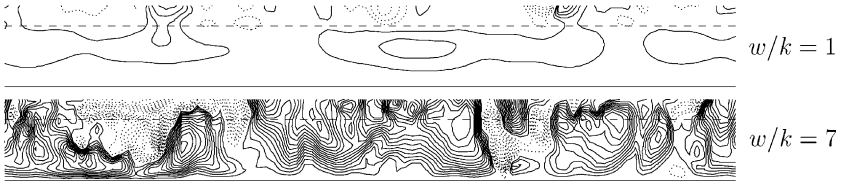


Fig. 12. Contours of instantaneous normal velocity in $z$-, $y$-planes, upstream of an element. Solid line, bottom wall, dashed line plane of the crests. Increments 0.02 (—) positive, (···) negative.

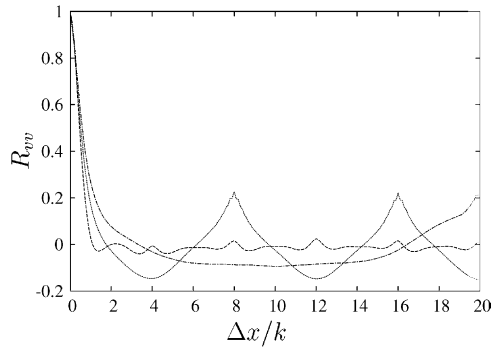


Fig. 13. Two=point correlation coefficients at $y^+ \simeq 10$ in streamwise direction. (- - -) $w/k = 3$; (···) $w/k = 7$; (– – –) $w/k = 19$.

of the vertical motion. Further, since the magnitudes of the peaks for $w/k = 7$ and $w/k = 19$ are identical, to a first approximation we can assume that the elements are virtually isolated when $w/k$ is equal to or exceeds $w/k = 7$.

To show how the vorticity field is perturbed by the square bars, instantaneous isosurfaces of $\omega_y (\equiv \partial u/\partial z - \partial \omega/\partial x)$ were computed (Fig. 14). For $w/k = 1$, the contours are parallel to the plane of the crests and similar to those over a smooth wall, except that they are shorter in $x$. While for $w/k = 1$, positive and negative contours alternate regularly in $z$ as over a smooth wall, for $w/k = 7$, the vorticity field is more complex. In fact, the fluctuations of $v$ and $w$, due to the "splashing" effect occurring near the leading edge of an element, lift the structures and increase their width in $z$. This is in agreement with the DNS by Ikeda and Durbin (2002).

To quantify the outward motion due to the roughness, the correlation $\langle \rho_{vv}(x_0) \rangle = \langle v(x_0)v(x) \rangle / (v'(x_0)v'(x))$ was computed (Fig. 15). For a smooth wall, the contours of $\rho_{vv}$ are elongated in $x$. Given that, the streaks gradually lift-up, oscillate and finally break down, it is not unreasonable that $v$ remains correlated over some streamwise distance. The contours for $w/k = 1$ are somewhat similar to those for the smooth wall even if they are less elongated. As for the $u$ contours, there are qualitative similarities despite quantitative differences between the smooth wall and a rough wall with $w/k = 1$. As $w/k$ increases, the contours depart from those over a smooth surface, and for $x = x_b$ and $x = x_c$ the $y$ extent of the correlation is even larger than that in $x$. In particular, near the leading edge, the $y$ extent of the correlation is largest and we expect that this is where ejections out of the cavity are more likely to occur (this is further corroborated by a quadrant analysis carried out by Leonardi (2002)). No significant differences are observed at $x = x_a$, $x_c$ for $w/k = 19$ and $w/k = 7$. As for $w/k \geqslant 7$, separation occurs over the crests (Leonardi et al., 2003).

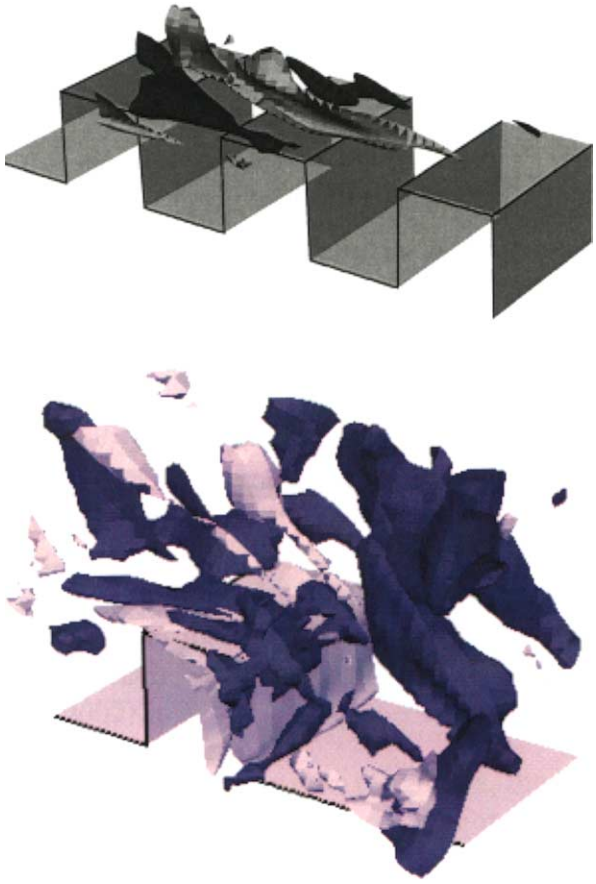

Fig. 14. Contours of instantaneous $\omega_y$. Top: $w/k = 1$, bottom: $w/k = 7$ Flow is right to left. Dark $\omega_y = -4$, light $\omega_y = 4$.

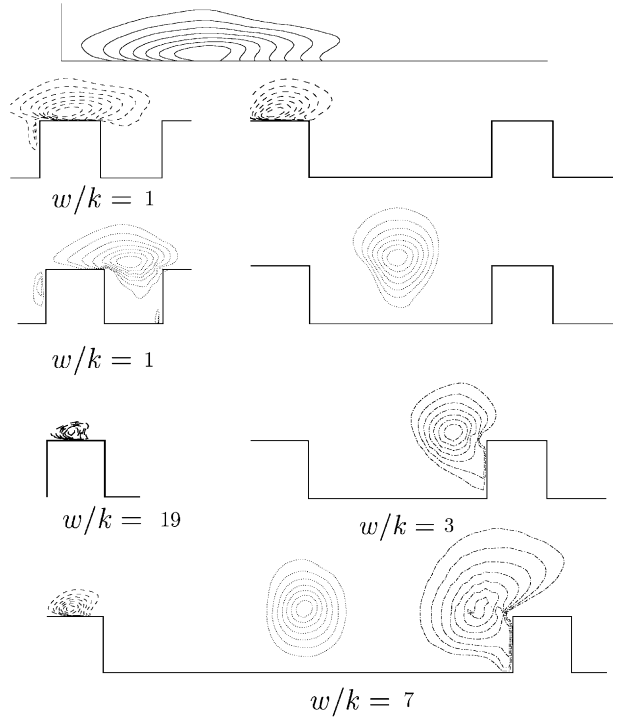


Fig. 15. Two-point $v$-correlations in the $(x, y)$-plane $\rho_{vv}(\mathbf{x_0})$, $y^+ = 6$. Contour levels range from 0.3 to 1 (increment is 0.1). Top, smooth wall (—); (- - -) $x = x_a$; (···) $x = x_b$; (– – –) $x = x_c$. Flow is left to right.

the correlation contours (at $x = x_a$) closely resembling the recirculation region over the crest.

## 7. Anisotropy invariants

An estimate of the overall anisotropy is in the Reynolds stress anisotropy tensor $b_{ij} = \langle u_i u_j \rangle / \langle u_i u_i \rangle - \delta_{ij}/3$ (Lumley, 1978). Here, $\langle u_i u_i \rangle$ is twice the turbulent kinetic energy, (where $u_1$, $u_2$, $u_3 \equiv u$, $v$,$w$), and repeated index summation is implied. $\delta_{ij}$ is the Kronecker delta function. The tensor $b_{ij}$ is symmetric, traceless and is bounded by the inequalities $-1/3 \leqslant b_{ij} \leqslant 2/3$. For isotropic turbulence, each stress contributes as one third of the total turbulent kinetic energy so that each $b_{ij}$ should be zero. For the smooth channel flow, the longitudinal turbulence intensity is much larger than the other components, hence $b_{11}$ is positive and $b_{22}$ and $b_{33}$ are negative (Fig. 16). For $w/k = 1$, the distributions are closer to those on the smooth wall ones with a small reduction of $b_{11}$ and a small increase of $b_{22}$ and $b_{33}$. As $w/k$ increases, the intensity of the spanwise and normal-wall velocity fluctuations increases and, for $w/k = 7$, $b_{11}$ is minimum at $y/h \simeq 0.2$. Since $b_{ii} = 0$, $b_{22}$ and $b_{33}$ are maximum at the same location. As all the $b_{ij}$'s are closer to zero with respect to the smooth wall, roughness enhances isotropy. Further, whereas the $b_{ij}$'s vary with $y$ for the smooth wall, for $w/k = 3$, 7 they are approximately constant in $y$, suggesting that the ratios between $\langle u^2 \rangle$, $\langle v^2 \rangle$ and $\langle w^2 \rangle$ are approximately constant with respect to $y$.

A convenient method for comparing the overall anisotropy is given by the function $F = 1 + 9\mathrm{II} + 27\mathrm{III}$, where $\mathrm{II}[\equiv -b_{ij}b_{ji}/2]$ and $\mathrm{III}[\equiv b_{ij}b_{jk}b_{ki}/3]$ are the second and third invariants of $b_{ij}$. The function $F$ is a measure of the approach to either two-component turbulence ($F = 0$) or a three-component isotropic state ($F = 1$). Over a smooth wall, isotropy is quite poor near the wall, due to the organisation associated with the quasi-longitudinal structures, and only approximately satisfied in the centreline region. As the three stresses do not coincide, $F$ is smaller than 1. Fig. 17 shows that near the rough wall, the isotropy is definitely increased ($y = 0$ coincides with the plane of the crests). The maximum value of $F$ is shifted beyond the centreline ($y/h = 1$). For large values of $w/k$, a region of constant $F$ extends over about $3k$. A comparison of $F$ at the same $y$ for $y > 3k$ could lead to the conclusion of Mazouz et al. (1998) (and in disagreement with what is generally found in the literature) that roughness increases the anisotropy. In fact, at the geometrical centreline of $w/k = 7$, the differences between $\langle u^2 \rangle$ and $\langle v^2 \rangle$ or $\langle w^2 \rangle$ are larger than for a smooth channel. This is due to the upward shift produced by the roughness, and not a genuine impairment in isotropy, the peak in $F$ having about the same intensity and occurring at about $y/h = 1.4$. This is further corroborated by Fig. 17b where the function $F$ is plotted versus $(y_{\max} - y)/h$, where $y_{\max}$ is the location

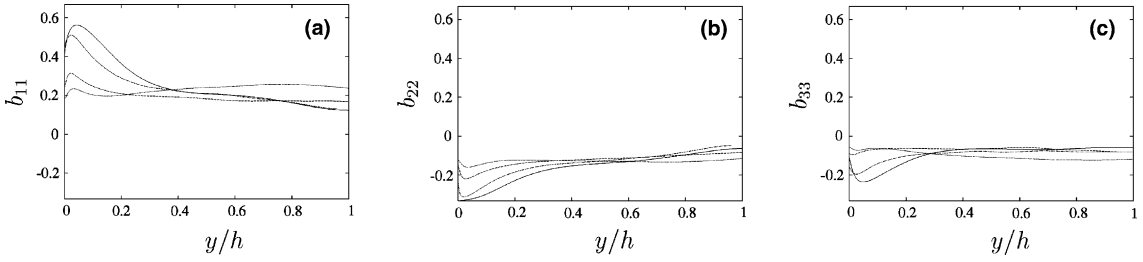


Fig. 16. Components of the anisotropy tensor $b_{ij}$ averaged with respect to time $x$ and $z$. (—) Kim et al. (1987), (– – –) $w/k = 1$, (- - -) $w/k = 3$, (· · ·) $w/k = 7$.

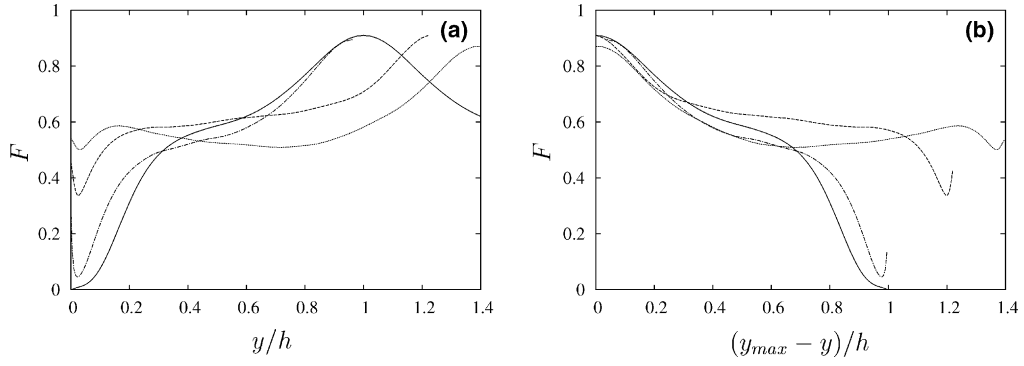


Fig. 17. Invariant $F = 1 + 9\mathrm{II} + 27\mathrm{III}$ for square bars roughness: symbols as in Fig. 16; in (b) $y_{\max}$ is the location of the maximum $F$.

where $F$ is maximum. For $y \simeq y_{\max}$ the value of $F$ is about the same for all the surfaces. For larger values of $(y_{\max} - y)/h$, i.e. as the wall is approached, isotropy is better approximated above the rough wall, and in particular for $w/k = 7$. The case $w/k = 1$ is, as expected from the previous figures, closest to the smooth wall.

## 8. Conclusions

The present direct numerical simulations indicate that near a rough wall, made up of transverse square bars, the structures are less elongated than over a smooth wall. As $w/k$ increases, the coherence is reduced in the streamwise direction with a minimum for $w/k = 7$. On the other hands the structures appear larger in the spanwise direction. The changes in the structures may be related to the strength of outward ejections of fluid from the cavities; this strength reaches its maximum for $w/k = 7$. The increased intensity of the wall-normal velocity fluctuations is coupled to an increased strength in the spanwise velocity fluctuations, which is difficult to measure reliably in experiments. On the other hand, the streamwise velocity fluctuation is not very different to that on a smooth wall. Hence isotropy, close to the wall, is better approximated over a rough than a smooth wall. The dependence on $w/k$ is very strong; for very small values of $w/k$, structures and turbulent intensities resemble those over a smooth wall. For $w/k = 3$, the effect of the wall extends up to about $2k$ above the plane of the crests, while, for $w/k = 7$, the distance is as large as $5k$. The ratio $w/k = 7$ corresponds to that for which with the roughness function $\Delta U^+$ is largest (Leonardi et al., 2003). For larger values of $w/k$, the normal wall motion induced by the roughness is confined to smaller regions, and the overlying flow is closer to that above a smooth wall.

## Acknowledgements

We acknowledge the support of the Australian Research Council, and the Ministero dell' Istruzione (MPI 60% grant), dell' Università e della Ricerca and Centra di Eccellenza di Meccanica Computazionale (CEMeC), Politecnico di Bari. Discussions with P.-Å. Krogstad and H.I. Anderson were appreciated.

## References

Ashrafian, A., Anderson, H.I., 2003. DNS of turbulent flow in a rod-roughened channel. In: Kasagi, N., Eaton, J.K., Friedrich, R., Humphrey, J.A.C., Leschziner, M.A., Miyauchi, T. (Eds.), Proceedings of the Turbulent and Shear Flow Phenomena 3, Sendai, Japan, vol. I, pp. 117–123.

Bakken, O.M., Krogstad, P.A., 2003. Stress measurements in a rough wall channel flow using variable angle method of calibration for X-probes. In: Kasagi, N., Eaton, J.K., Friedrich, R., Humphrey, J.A.C., Leschziner, M.A., Miyauchi, T. (Eds.), Proceedings of the Turbulent and Shear Flow Phenomena 3, Sendai, Japan, vol. I, pp. 105–111.

Cantwell, B.J., 1981. Organized motion in turbulent flow. Annu. Rev. Fluid Mech. 13, 437–515.

Cui, J., Patel, V.C., Lin, C.-L., 2003. Large-eddy simulation of turbulent flow in a channel with rib roughness. Int. J. Heat Fluid Flow 24, 372–388.

Djenidi, L., Elavarasan, R., Antonia, R.A., 1999. The turbulent boundary layer over transverse square cavities. J. Fluid Mech. 395, 271–294.

Fadlun, E.A., Verzicco, R., Orlandi, P., Mohd-Yusof, J., 2000. Combined immersed boundary finite-difference methods for three-dimensional complex flow simulations. J. Comput. Phys. 161, 35–60.

Grass, A.J., Stuart, R.J., Mansour-Thehrani, M., 1993. Common vortical structure of turbulent flows over smooth and rough boundaries. AIAA J. 31, 837–846.

Ikeda, T., Durbin, P.A., 2002. Direct simulations of a rough-wall channel flow. Report No. TF 81, Department of Mechanical Engineering, Stanford University, Stanford, CA.

Kim, J., Moin, P., Moser, R., 1987. Turbulence statistics in fully developed channel flow at low Reynolds number. J. Fluid Mech. 177, 133–166.

Kline, S.J., Reynolds, W.C., Schraub, F.A., Runstadler, P.W., 1967. The structure of turbulent boundary layers. J. Fluid Mech. 30, 741–773.

Krogstad, P.-Å., Antonia, R.A., 1994. Structure of turbulent boundary layers on smooth and rough walls. J. Fluid Mech. 277, 1–21.

Krogstad, P.-Å., Antonia, R.A., Browne, L.W.B., 1992. Comparison between rough- and smooth-wall turbulent boundary layers. J. Fluid Mech. 245, 599–617.

Le, H., Moin, P., Kim, J., 1997. Direct numerical simulation of turbulent flow over a backward-facing step. J. Fluid Mech. 330, 349–374.

Leonardi, S., 2002. Turbulent channel flow with roughness: direct numerical simulations. PhD thesis, University of Rome, La Sapienza.

Leonardi, S., Orlandi, P., Smalley, R.J., Djenidi, L., Antonia, R.A., 2003. Direct numerical simulations of turbulent channel flow with transverse square bars on one wall. J. Fluid Mech. 491, 229–238.

Liu, O.K., Kline, S.J., Johnston, J.P., 1966. An experimental study of turbulent boundary layers on rough walls. Report MD-15, Department of Mechanical Engineering, Stanford University.

Lumley, J.L., 1978. Computational modeling of turbulent flows. Adv. Appl. Mech. 18, 123–176.

Mazouz, A., Labraga, L., Tournier, C., 1998. Anisotropy invariants of reynolds stress tensor in a duct flow and turbulent boundary layer. J. Fluid Eng. 120, 280–284.

Orlandi, P., 2000. Fluid Flow Phenomena: A Numerical Toolkit. Kluwer, Dordrecht.

Perry, A.E., Schofield, W.H., Joubert, P.N., 1969. Rough wall turbulent boundary layers. J. Fluid Mech. 37, 383–413.

Robinson, S.K., 1991. Coherent motions in the turbulent boundary layer. Annu. Rev. Fluid Mech., 601–639.

Wood, D.H., Antonia, R.A., 1975. Measurements of a turbulent boundary layer over a d-type surface roughness. J. Appl. Mech. 42, 591–597.